PHYSICAL REVIEW B **80**, 085303 (2009)

Quantum oscillations in a topological insulator $Bi_{1-x}Sb_x$

A. A. Taskin and Yoichi Ando
Institute of Scientific and Industrial Research, Osaka University, Osaka 567-0047, Japan
(Received 26 May 2009; revised manuscript received 14 July 2009; published 6 August 2009)

We have studied transport and magnetic properties of $Bi_{1-x}Sb_x$, which is believed to be a topological insulator—a new state of matter where an insulating bulk supports an intrinsically metallic surface. In nominally insulating $Bi_{0.91}Sb_{0.09}$ crystals, we observed strong quantum oscillations of the magnetization and the resistivity originating from a Fermi surface which has a clear two-dimensional character. In addition, a three-dimensional Fermi surface is found to coexist, which is possibly due to an unusual coupling of the bulk to the surface. This finding demonstrates that quantum oscillations can be a powerful tool to directly probe the novel electronic states in topological insulators.

DOI: 10.1103/PhysRevB.80.085303 PACS number(s): 71.18.+y, 71.70.Di, 73.43.−f, 85.75.−d

I. INTRODUCTION

Bi and $Bi_{1-x}Sb_x$ alloys have been "gold mines" of modern solid-state physics for over seven decades.[1–8] The discovery of quantum oscillations itself has been made on pure Bi as long ago as 1930. The anomalously large diamagnetism in Bi was a fundamentally important problem[1] and prompted the application of the Dirac theory to solid states[1,2] in the 1960s. Also, $Bi_{1-x}Sb_x$ is known as one of the best thermoelectric materials[3] and consequently has been studied in great detail. As a result, Bi and $Bi_{1-x}Sb_x$ have been thought to be very well understood. Yet, a new twist came recently[9–21] from new ideas about topological phases in condensed matter,[9–15] namely, it has been realized that $Bi_{1-x}Sb_x$ in the insulating regime ($0.07<x<0.22$) is a "topological insulator" (TI) that belongs to a nontrivial Z_2 topological class.[10] Since the vacuum belongs to a trivial topological class, a smooth transition from a TI to the vacuum is possible only by closing the energy gap along the way, making the surface of a TI to be intrinsically conducting. Intriguingly, those metallic surface states are expected to be spin filtered, obey Dirac-type energy dispersion, and be topologically protected.[9–12]

In the past, a metallic behavior has always been observed at low temperature in $Bi_{1-x}Sb_x$, namely, its resistivity has never presented a true divergence in the zero-temperature limit even in the insulating doping range where a bulk energy gap opens.[3] The origin of this metallic state at low temperature has never been fully understood and was mainly attributed to imperfections of measured crystals, in particular, to the formation of an impurity band within the bulk energy gap. On the other hand, recent angle-resolved photoemission spectroscopy (ARPES) studies on its cleaved (111) trigonal surface have revealed that the energy dispersions of the surface states possess the distinctive character to qualify this material as a topological insulator,[17–21] so it is natural to ask whether the low-temperature metallic behavior of "insulating" $Bi_{1-x}Sb_x$ has anything to do with the topological surface state. In the present work, to directly address this question, we measure quantum oscillations (QOs) in nominally insulating $Bi_{0.91}Sb_{0.09}$ crystal to differentiate a coherent electronic transport on a fully developed Fermi surface (FS) from an incoherent transport within an impurity band.

II. EXPERIMENTAL DETAILS

$Bi_{1-x}Sb_x$ crystals were grown from a stoichiometric mixture of 99.9999% purity Bi and Sb elements by a zone melting method. The homogenization of $Bi_{1-x}Sb_x$ microstructure was achieved by multiple (~100 times) remelting of the boule. The last run for each growth was done at a very low rate (≤0.2 mm/h) to avoid constitutional supercooling and the resulting segregation of the solid solution. All grown crystals were easily cleaved along the (111) plane, revealing flat, shiny surfaces.

To prepare samples suitable for transport and magnetic measurements, crystals were aligned using the x-ray Laue analysis and cut along the principal axes. The actual composition of grown crystals and their purity were checked by the inductively coupled plasma atomic-emission spectroscopy (ICP-AES) analysis, which confirmed that the composition of grown $Bi_{1-x}Sb_x$ was close to the nominal value and that the concentration of any impurity atoms was less than the sensitivity threshold (~10^{21} m^{-3}).

The resistivity was measured by a standard four-probe method on a rectangular sample with the size of approximately $1.5\times0.2\times0.1$ mm^3. Six ohmic contacts were made with a silver paste and cured at room temperature. The electric current was directed along the C_3 axis, and the magnetic field was applied along the C_2 axis. The magnetic-field dependences of both the longitudinal and transverse resistivities, ρ_{xx} and ρ_{xy}, were measured by sweeping the magnetic field from +14 to −14 T and back to +14 T at fixed temperatures.

For the de Haas–van Alphen (dHvA) measurements, a sample of approximately cubic shape and the mass of ~80 mg was cut along the principal crystallographic axes from the same $Bi_{0.91}Sb_{0.09}$ crystal as was used for the resistivity measurements. The dc magnetization M was measured in magnetic fields up to 1 T at fixed temperatures in the range from 2 to 40 K using a commercial Quantum Design SQUID magnetometer. Quasiequilibrium measurement conditions allowed us to observe even a weak modulation of the magnetization in fields as low as 0.08 T. The dHvA oscillations of M/B were obtained from the magnetic-field dependence of M, measured for different orientations of the sample with respect to the magnetic field.

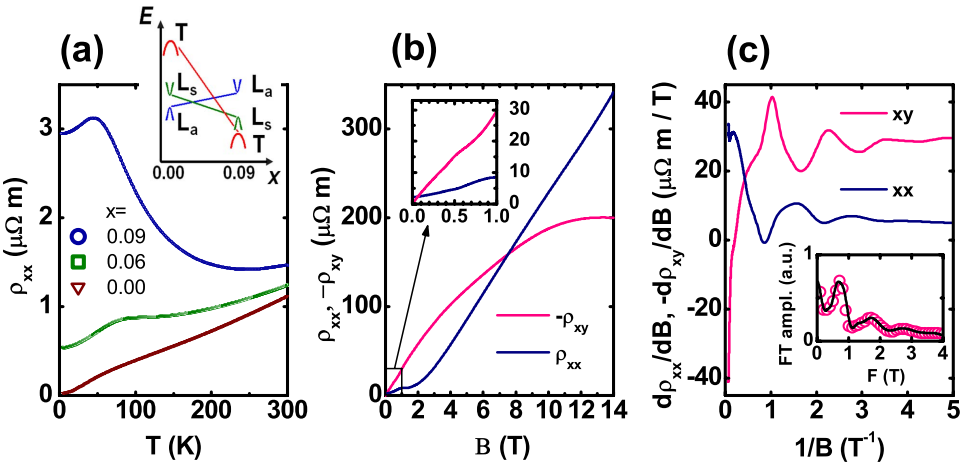

FIG. 1. (Color online) (a) Temperature dependences of ρ_{xx} for $x=0.00$, 0.06, and 0.09. Inset shows a diagram of the evolution of the energy bands in $Bi_{1-x}Sb_x$ upon doping. (b) Magnetic-field dependences of ρ_{xx} and $-\rho_{xy}$ in $Bi_{0.91}Sb_{0.09}$ at 1.4 K. (c) Derivatives of $\rho_{xx}(B)$ and $-\rho_{xy}(B)$ vs B^{-1}. Inset shows the FT spectrum of the $-\rho_{xy}$ oscillations.

III. MAGNETOTRANSPORT PROPERTIES

The temperature dependences of the resistivity, $\rho_{xx}(T)$, for three high-quality $Bi_{1-x}Sb_x$ crystals with increasing Sb concentration, $x=0.00$, 0.06, and 0.09, are shown in Fig. 1(a). A qualitative change from a metallic behavior with positive slope $d\rho/dT>0$ to an insulatorlike behavior is clearly seen between $x=0.06$ and 0.09. This indicates that, at $x=0.09$, an energy gap for charge carriers fully opens, in agreement with recent ARPES measurements[19–21] as well as the well-established evolution of the energy bands in $Bi_{1-x}Sb_x$ upon doping.[3,5] The change from the semimetal nature in pure Bi ($x=0.00$), resulting from an overlap of the valence and conduction bands at different points in the Brillouin zone (BZ), to the bulk-insulator nature at $x=0.09$ with a direct gap at the zone boundary is schematically depicted in the inset of Fig. 1(a). Despite the upturn in the resistivity below 200 K, the sample with $x=0.09$ shows a metallic behavior below 40 K, even though the resistivity value is about 100 times larger than in pure Bi in the zero-temperature limit.

Figure 1(b) shows that both ρ_{xx} and ρ_{xy} of the $x=0.09$ sample change strongly with the magnetic field B at 1.4 K. The $\rho_{xx}(B)$ shows an almost linear increase above ~2 T and, at 14 T, it is ~170 times larger than at 0 T. The $\rho_{xy}(B)$, on the other hand, is almost linear at low fields and shows a saturation around 14 T. The negative slope of $\rho_{xy}(B)$ at $B=0$ T suggests that the main carriers in the sample are electrons [note that $-\rho_{xy}(B)$ is plotted in Fig. 1(b)]. The Hall coefficient R_H estimated from the slope is -3.5×10^{-5} m^3/C implying that the concentration of electrons in the sample is on the order of $|1/eR_H|\approx1.8\times10^{23}$ m^{-3}. At low fields, both $\rho_{xx}(B)$ and $\rho_{xy}(B)$ show a weak modulation in the magnetic field (more clearly seen in the inset). Their derivatives with respect to B plotted vs $1/B$ [Fig. 1(c)] reveal clear Shubnikov-de Haas (SdH) oscillations in magnetic fields below ~2 T, which unambiguously indicate that the low-temperature metallic behavior in nominally insulating $Bi_{1-x}Sb_x$ is *not* due to some impurity band but owes itself to well-defined Fermi surfaces. The Fourier transform (FT) of $d\rho_{xy}/dB$ [Fig. 1(c) inset] yields the power spectrum with the leading frequency of 0.67 T. Such an observation of QOs in a nominally insulating material is surprising, and we elucidate their origin in the following.

IV. THE DE HAAS–VAN ALPHEN EFFECT

The dHvA effect, which we also observe in our $Bi_{0.91}Sb_{0.09}$ crystal, is another way of probing the Fermi surface. This effect is manifested in magnetization which is a very straightforward thermodynamic property. An example of oscillations of the magnetic susceptibility M/B measured at 2 K with the magnetic-field direction lying in the binary plane (perpendicular to the C_2 axis) at different angles θ is shown in Fig. 2(a), where a complex structure of the oscillations as well as changes in their amplitudes and periods are clearly seen. Shown in Fig. 2(b) is a schematic representation of the BZ, three main axes, positions of high symmetry points, and geometry of the present experiment. The Fourier analysis is applied to all measured data to obtain quantitative information, and Fig. 2(c) shows, as an example, the decomposition of magnetic oscillations into a set of constituents for $B\|C_1$ axis. The experimental data are shown at the bottom by symbols. The inset of Fig. 2(c) displays the FT spectra for four measured temperatures; several frequencies can be readily distinguished, and up to the fifth harmonic of the lowest frequency f_1 can be identified at 2 K, indicating a high degree of coherence.[22]

The angular dependence of the FT amplitude of the main peak f_1 for magnetic fields in the binary plane is shown in Fig. 3. This amplitude exhibits a very sharp decrease by as much as four orders of magnitude when the magnetic-field direction approaches the bisectrix plane (perpendicular to the C_1 axis), as if carriers cannot move perpendicular to this plane to make Larmor orbit. This angular dependence is the first indication of a two-dimensional (2D) nature of the corresponding FS. On the other hand, the amplitude of the second peak f_2 seems to remain finite at $\theta=0$, suggesting that f_2 originates from a three-dimensional (3D) FS.

V. THE FERMI SURFACES

Since the frequencies of QOs, F, are directly related to the Fermi-surface cross-sections via the Onsager relation $F=(\hbar c/2\pi e)A$, where A is the area of an extremal cyclotron orbit, the shape and size of the FS can be obtained from the angular dependences of F measured within the three main crystallographic planes. To separate the FT peaks associated

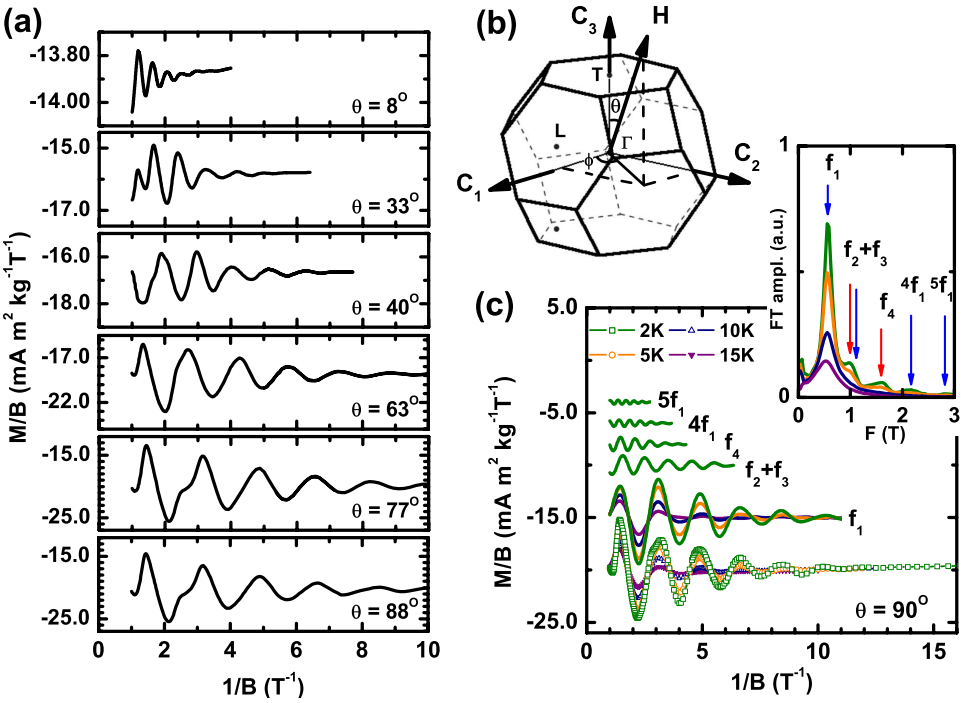

FIG. 2. (Color online) (a) Example of the angular dependence of the dHvA oscillations in $Bi_{0.91}Sb_{0.09}$ at 2 K for magnetic fields in the binary plane (i.e., θ is varied, while $\phi=0°$ is fixed). (b) Schematic picture of the bulk Brillouin zone of $Bi_{1-x}Sb_x$ and the geometry of the experiment. (c) Example of the decomposition of the raw M/B data (shown by symbols at the bottom) into a set of oscillatory parts (shown by straight lines); inset shows the FT spectra at 2, 5, 10, and 15 K for $\theta=90°$ and $\phi=180°$.

with different Fermi surfaces, the angle-dependent FT spectra in the binary, trigonal, and bisectrix planes (which are perpendicular to the C_2, C_3, and C_1 axes, respectively) have been mapped [Figs. 4(a)–4(c)]. By following the change in position of individual peaks in the spectra with changing angle, as shown in Figs. 4(a)–4(c) by lines, it is easy to sort out the evolution of each peak, which allows us to plot the angular dependences of all periods $P=1/F$ of the dHvA oscillations within the three main planes, as shown in Fig. 4(d) by symbols. The period of the SdH oscillations [Fig. 1(c)] is also shown by a filled circle in Fig. 4(d). The branches in Fig. 4(d) are separated into two sets: in the binary plane $(\bar{C}_1-C_3-C_1)$, two branches (shown by open circles) are symmetrical with respect to the positive (C_1) and negative $(\bar{C}_1)$ axes direction and have a minimum (in fact, approaching zero) at exactly $\theta=0°$, while the other two branches (shown by open triangles) are slightly shifted with respect to $\theta=0°$.

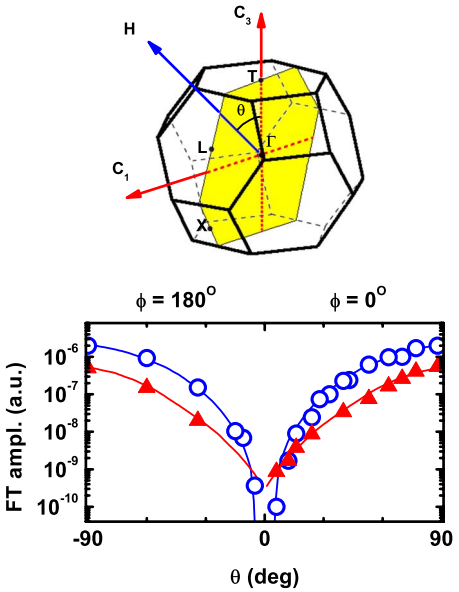

FIG. 3. (Color online) The amplitudes of the two Fourier components with frequencies f_1 (open circle) and f_2 (filled triangle) obtained from the dHvA oscillations for the field direction in the binary plane (marked by yellow).

Taking into account all three planes, the angular dependences of the observed periods point to a coexistence of 2D and 3D Fermi surfaces: the 2D one is a circle of radius $k_F=4.15\times10^7$ m^{-1} lying in the bisectrix plane (perpendicular to the C_1 axis). Since there is no obvious 2D structure along the bisectrix plane in bulk $Bi_{1-x}Sb_x$, we tentatively associate the observed 2D Fermi "circle" to the surface state on the bisectrix $(2\bar{1}\bar{1})$ surface, and there can be six equivalent surfaces by symmetry. The size of this circle corresponds to the surface charge-carrier concentration $n_s=k_F^2/4\pi=1.4\times10^{14}$ m^{-2}, if the surface state is spin filtered; it will be twice as large, if the state is not spin filtered. Branches calculated in this model are shown in Fig. 4(d) by thick (blue) solid lines, which match the data almost completely. The 3D FS is a set of three ellipsoids, located at the L points of the BZ with semiaxes $a=2.7\times10^8$ m^{-1}, $b=1.3\times10^8$ m^{-1}, and $c=2.3\times10^7$ m^{-1} that are approximately along C_1, C_2, and C_3, respectively; to be precise, the ellipsoids are tilted by approximately +6° in the binary planes [see Fig. 4(e)]. The size of each ellipsoid corresponds to the bulk charge-carrier concentration of $abc/3\pi^2=2.7\times10^{22}$ m^{-3}. In total, three ellipsoids give $\sim8.1\times10^{22}$ m^{-3}. Calculated branches for those 3D states are shown in Fig. 4(d) by thin (red) solid lines, which, again, match the data very well. The shapes of the 2D and 3D FSs are schematically shown in Fig. 4(e).

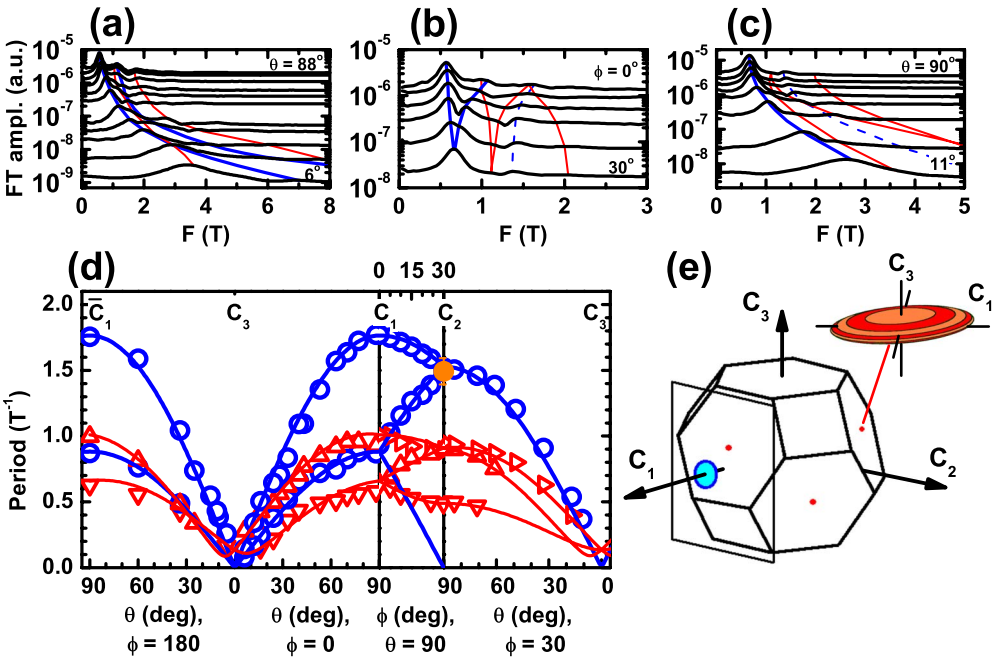

FIG. 4. (Color online) (a)–(c) Evolution of the FT components of the dHvA oscillations upon rotating the magnetic field within the (a) binary, (b) trigonal, and (c) bisectrix planes. All spectra in (a) and (c) are naturally shifted along the ordinate axis, owing to the strong θ dependence of the amplitude (see Fig. 3), while the shift in (b) is obtained by dividing each spectrum by $\sim(1.5)^{\Delta\phi/5^\circ}$. The lines are guides to the eyes, and the dashed lines denote those peaks that are not independent but come from higher harmonics or interference of independent frequencies. (d) Angular dependences of $P(=1/F)$ within the three main planes; experimental data, corresponding to the peaks in (a)–(c), are shown by symbols. Thick (blue) and thin (red) solid lines are the fits using the model considering the 2D and 3D Fermi surfaces, respectively (see text). (e) Schematic picture of the surface and bulk FSs and their positions in the BZ.

VI. DISCUSSION

An important parameter that can be extracted from the dHvA oscillations is the cyclotron mass m_c. The temperature dependences of the oscillation amplitude for different angle θ (with fixed $\phi=0^\circ$) are shown in Fig. 5(a), where fittings of the data to the standard Lifshitz-Kosevich theory[23] are shown by solid lines.[24] This analysis gives the angular dependence of m_c associated with the surface states as shown in Fig. 5(b). Two prominent features are readily recognized: first, the absolute value of m_c in the magnetic field perpendicular to the surface ($\theta=90^\circ$) is extremely small, measuring only $0.0057m_e$ (m_e is the free-electron mass), which is smaller than the cyclotron mass in pure Bi for any direction. Such a small m_c is the reason why it is possible to observe pronounced oscillations at relatively low magnetic fields. Second, $m_c(\theta)$ diverges at $\theta=0^\circ$ and shows the $1/\sin\theta$ dependence, that is, characteristic of a 2D FS, giving unambiguous evidence for the 2D nature.[25]

Once m_c is known, the scattering time τ is obtained by analyzing how M/B changes with B^{-1} at fixed temperatures. Figure 5(c) shows the Dingle plots,[23] which yields the Dingle temperature $T_D(=\hbar/2\pi\tau k_B)$ for the same field directions as in Fig. 5(a). All curves show linear slopes and for all angles the same T_D of 6.7 K (which corresponds to $\tau\approx 1.8\times10^{-13}$ s) is obtained. This is surprisingly low effective temperature for an alloy with this doping concentration.[23] Since the Fermi velocity v_F can be approximated by $v_F=\hbar k_F/m_c\approx 8.5$

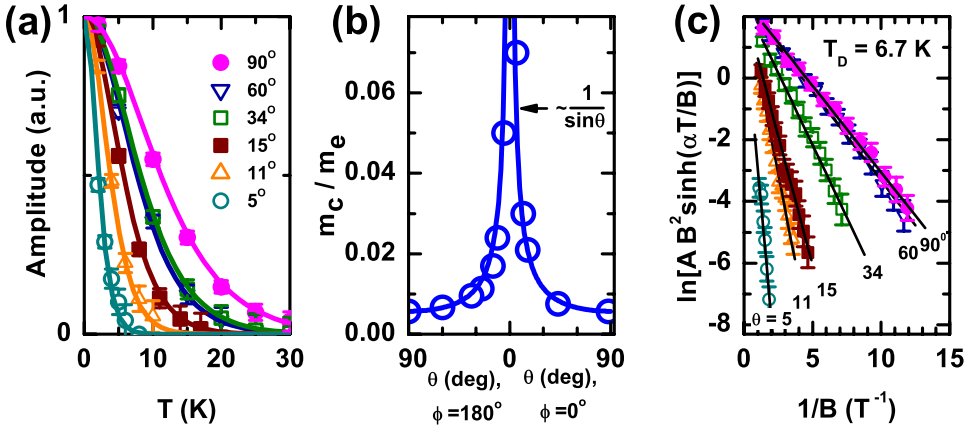

FIG. 5. (Color online) (a) Temperature dependences of the dHvA amplitudes measured at a fixed magnetic field below the quantum limit within the binary plane. Solid lines are the fits to the standard Lifshitz-Kosevich formula. (b) Angular dependence of m_c signifying the unambiguous 2D nature. (c) Dingle plots yielding the same Dingle temperature for all magnetic-field directions, A is the dHvA amplitude and $\alpha=14.7(m_c/m_e)$[T/K].

$\times 10^5$ m/s, the mean free path ℓ on the surface is estimated as $\ell = v_F \tau \approx 150$ nm, which is comparable to the de Broglie wavelength $\lambda = 2\pi/k_F \approx 150$ nm for the 2D FS. In passing, we note that our samples have a rectangular shape and four of the surfaces were cut along the C_3 axis with a wire saw; hence, those four surfaces are actually a collection of locally flat minisurfaces with various orientations. Naturally, some of the minisurfaces are perpendicular to the C_1 axis, and as long as their extent is larger than ℓ, they can produce QOs.

Let us now combine the dHvA results on $Bi_{0.91}Sb_{0.09}$ with the transport data. The bulk FS gives the total number of charge carriers, n_{bulk}, of $\sim 8.1 \times 10^{22}$ m^{-3}, which is close to the value $\sim 1.8 \times 10^{23}$ m^{-3} estimated from R_H. This means that the observed bulk ellipsoids must be electron pockets. The band scheme[3] of $Bi_{1-x}Sb_x$ dictates that those electron pockets be located at the three L points in the BZ, which is consistent with our model to fit the data in Fig. 4(d). The surface FS is most likely a hole pocket because the measured R_H gives an overestimated carrier concentration, which is naturally understood if there is a partial cancelation of the Hall effect from the electron and hole contributions.

We note that n_{bulk} obtained from the dHvA effect is much larger than the possible concentration of impurities, donors or acceptors, of $\sim 10^{21}$ m^{-3} (estimated from the ICP-AES analysis) in our $Bi_{0.91}Sb_{0.09}$ crystal. Then, why is the Fermi level in the bulk of $Bi_{0.91}Sb_{0.09}$ not located in the gap but goes into the conduction band, giving a rather appreciable electron concentration? We speculate that this is due to a coupling of the bulk FS to the surface FS that causes an intrinsic self-doping, but the actual mechanism is to be elucidated. Also, the amplitude of the dHvA oscillations from the 2D FS appears to be orders of magnitude larger than what is expected if each surface hole contributes a magnetic moment of $\sim \hbar e/m_c c$; this puzzle will probably be resolved if the unique properties of the surface states of a TI, the Dirac-type[26] and spin-filtered nature and the topological protection, are properly taken into account.[27] An alternative scenario that may account for the large dHvA amplitudes from the 2D FS and the unusual electron-hole coupling would be a formation of a 2D cylindrical FS perpendicular to the bisectrix planes within the bulk BZ; however, this is probably too exotic, given the 3D crystal structure of $Bi_{1-x}Sb_x$. Clearly, there is a lot to understand about the macroscopic properties of topological insulators, and the availability of the powerful tool of quantum oscillations demonstrated here promises a vast possibility for future research.

VII. CONCLUSION

We have observed both the SdH and dHvA oscillations in nominally insulating $Bi_{0.91}Sb_{0.09}$, which is believed to be a topological insulator. The FS that gives the leading contribution to the quantum oscillations is found to possess an unambiguous 2D character, suggesting that it is due to a topologically protected surface-state characteristic of a topological insulator. Since it is a common sense in surface physics that metallic surface states are very fragile against disturbances such as adsorption, it is surprising that a native surface state of a bulk material can be seen by transport and magnetization in ambient atmosphere, if the observed 2D FS is indeed due to the surface state. Intriguingly, the amplitude of the quantum oscillations associated with the 2D FS appears to be orders of magnitude larger than what is naively expected from the total number of surface carriers, which calls for better understanding of the nature of surface Dirac fermions.

ACKNOWLEDGMENTS

We thank M. Hagiwara, Y. Onuki, and S.-C. Zhang for helpful discussions. This work was supported by JSPS (KAKENHI Grants No. 19340078 and No. 2003004) and AFOSR (Grant No. AOARD-08-4099).

[1] H. Fukuyama and R. Kubo, J. Phys. Soc. Jpn. **28**, 570 (1970).
[2] P. A. Wolff, J. Phys. Chem. Solids **25**, 1057 (1964).
[3] B. Lenoir, M. Cassart, J.-P. Michenaud, H. Scerrer, and S. Scherrer, J. Phys. Chem. Solids **57**, 89 (1996).
[4] V. S. Édel'man, Adv. Phys. **25**, 555 (1976).
[5] N. B. Brandt and E. A. Svistova, J. Low Temp. Phys. **2**, 1 (1970).
[6] K. Behnia, L. Balicas, and Y. Kopelevich, Science **317**, 1729 (2007).
[7] L. Li, J. G. Checkelsky, Y. S. Hor, C. Uher, A. F. Hebard, R. J. Cava, and N. P. Ong, Science **321**, 547 (2008).
[8] A. Banerjee, B. Fauqué, K. Izawa, A. Miyake, I. Sheikin, J. Flouquet, B. Lenoir, and K. Behnia, Phys. Rev. B **78**, 161103(R) (2008).
[9] L. Fu, C. L. Kane, and E. J. Mele, Phys. Rev. Lett. **98**, 106803 (2007).
[10] L. Fu and C. L. Kane, Phys. Rev. B **76**, 045302 (2007).
[11] J. E. Moore and L. Balents, Phys. Rev. B **75**, 121306(R) (2007).
[12] X.-L. Qi, T. L. Hughes, and S.-C. Zhang, Phys. Rev. B **78**, 195424 (2008).
[13] C. L. Kane and E. J. Mele, Phys. Rev. Lett. **95**, 146802 (2005).
[14] B. A. Bernevig, T. L. Hughes, and S.-C. Zhang, Science **314**, 1757 (2006).
[15] S. Murakami, S. Iso, Y. Avishai, M. Onoda, and N. Nagaosa, Phys. Rev. B **76**, 205304 (2007).
[16] M. König, S. Wiedmann, C. Brüne, A. Roth, H. Buhmann, L. W. Molenkamp, X.-L. Qi, and S.-C. Zhang, Science **318**, 766 (2007).
[17] J. C. Y. Teo, L. Fu, and C. L. Kane, Phys. Rev. B **78**, 045426 (2008).
[18] H.-J. Zhang, C.-X. Liu, X.-L. Qi, X.-Y. Deng, X. Dai, S.-C. Zhang, and Z. Fang, arXiv:0901.2762 (unpublished).
[19] D. Hsieh, D. Qian, L. Wray, Y. Xia, Y. S. Hor, R. J. Cava, and M. Z. A. Hasan, Nature (London) **452**, 970 (2008).
[20] D. Hsieh, Y. Xia, L. Wray, D. Qian, A. Pal, J. H. Dil, J. Osterwalder, F. Meier, G. Bihlmayer, C. L. Kane, Y. S. Hor, R. J. Cava, and M. Z. Hasan, Science **323**, 919 (2009).
[21] A. Nishide, A. Taskin, Y. Takeichi, T. Okuda, A. Kakizaki, T.

Hirahara, K. Nakatsuji, F. Komori, Y. Ando, and I. Matsuda, arXiv:0902.2251 (unpublished).
[22] L. M. Falicov and H. Strachowiak, Phys. Rev. **147**, 505 (1966).
[23] D. Schoenberg, *Magnetic Oscillations in Metals* (Cambridge University Press, Cambridge, 1984).
[24] Maxima, that are related to the crossing of the Fermi energy by Landau levels with higher occupation numbers, were chosen for this analysis to reduce contributions from frequencies other than f_1.
[25] The angular dependence $m_c(\phi)$ in the trigonal plane is also close to $\sim 1/\sin(90^\circ - \phi)$, but the span of ϕ is limited to $0^\circ - 30^\circ$ due to the crystal symmetry, precluding a divergence in $m_c(\phi)$.
[26] S. G. Sharapov, V. P. Gusynin, and H. Beck, Phys. Rev. B **69**, 075104 (2004).
[27] In magnetic fields, the Kramers degeneracy is lifted and a Zeeman gap opens in the topological surface state. But the surface can remain metallic as long as the Fermi level is located within the surface band.